Intrinsic Pink-Noise Multidecadal Global Climate Dynamics Mode

Woosok Moon, Sahil Agarwal, and J. S. Wettlaufer

Phys. Rev. Lett. **121**, 108701 — Published 4 September 2018

DOI: 10.1103/PhysRevLett.121.108701

An intrinsic pink-noise multi-decadal global climate dynamics mode

Woosok Moon,[1,2] Sahil Agarwal,[3] and J. S. Wettlaufer[3,4,2]

[1] *Department of Mathematics, Stockholm University 106 91 Stockholm, Sweden*
[2] *Nordita, Royal Institute of Technology and Stockholm University, SE-10691 Stockholm, Sweden*
[3] *Yale University, New Haven, USA*
[4] *Mathematical Institute, University of Oxford, Oxford, UK*

(Dated: July 19, 2018)

Understanding multi-decadal variability is an essential goal of climate dynamics. For example, the recent phenomenon referred to as the "global warming hiatus" may reflect a coupling to an intrinsic, pre-industrial, multi-decadal variability process. Here, using a multi-fractal time series method, we demonstrate that forty-two data sets of seventy-nine proxies with global coverage exhibit pink noise characteristics on multi-decadal time scales. To quantify the persistence of this behavior, we examine high-resolution ice core and speleothem data to find pink noise in both pre- and post-industrial periods. We examine the spatial structure with Empirical Orthogonal Function (EOF) analysis of the monthly-averaged surface temperature from 1901 to 2012. The first mode clearly shows the distribution of ocean heat flux sinks located in the eastern Pacific and the Southern Ocean, and has pink noise characteristics on a multi-decadal time-scale. We hypothesize that this pink noise multi-decadal spatial mode may resonate with externally-driven greenhouse gas forcing, driving large-scale climate processes.

A central question in contemporary climate science concerns the relative roles of natural climate variability and anthropogenic forcing. Indeed, understanding the detailed human effect on global temperature is highly complex due to the nonlinear interactions of anthropogenic forcing with natural climate variability on multiple timescales, many of which transcend a typical human lifetime. The recent phenomena referred to as the "global warming hiatus" [1–5] is a compelling example emphasizing the potential of such interactions. Understanding the coupling between natural multi-decadal climate variability and anthropogenic forcing is a fundamental aspect of climate dynamics.

Here we describe a framework for characterizing the dynamics of natural global climate variability on multi-decadal timescales [6–8]. There are many challenges associated with direct investigations of the physical and statistical characteristics of global observations on multiple timescales. First, the strong seasonal variability in observations, such as surface air temperature, hinders the detection of long-term spatiotemporal correlations [9–11]. Moreover, there is a substantial land-ocean contrast in seasonal variability, making it difficult to extract the influence of climate variability on global scales. Second, the maximum length of the available station-based observations is only approximately 100 years, which may be insufficient to statistically discern multi-decadal variability. At the same time, nonlinear interactions between natural and anthropogenic contributions to the multi-decadal variability found in these observations cannot be trivially disentangled. To overcome these obstacles, we analyze the data in a manner that enables us to exclude the contributions of the strong seasonality in the station-based observations. Thus, we detect global multi-decadal timescales corresponding to pink noise dynamics, defined as having a power spectrum $S(f) \propto f^{-\beta}$, with frequency f and $\beta \approx 1$, also generally termed $1/f$ noise when $0 < \beta < 2$ [e.g., 12–17]. Furthermore, we analyze high-resolution proxy data spanning at least several hundred years to detect the footprint of these dynamics and to differentiate between anthropogenic forcing and natural climate variability.

We study the statistical characteristics of the decadal and multi-decadal variability of Earth's climate by analyzing the Goddard Institute for Space Studies (GISS) monthly-averaged surface temperature data from 1901 to 2012 [18, 19], and proxy data, such as $\delta^{18}O$ and $\delta^{13}C$, from ice-cores and speleothems from forty-two paleoclimate datasets (see Table 1 of [20]). To examine the temporal dynamics of the data, we use Multi-Fractal Temporally Weighted Detrended Fluctuation Analysis (MF-TW-DFA) [11, 21]. This methodology captures the statistical dynamics (e.g., white noise, red noise, degree of correlation) on multiple time scales. The veracity of the approach has been demonstrated in various fields, such as the study of Arctic sea ice extent [11], sea ice velocity fields [22], and even in the detection of exoplanets, in all cases solely using the data with no a-priori modeling [23]. This approach produces a statistical measure called the fluctuation function, $F_q(s)$, each moment of which q, is assessed on multiple time scales s, as described in [11, 20, 21] in more detail. For intuition, one can think of the expectation value of $F_q(s)$ as the weighted sum of the auto-correlation function [e.g., 24]. The dominant time scales in a system are the those where $F_q(s)$ versus s changes slope and the individual slopes are associated with the statistical dynamics of a system.

First, we analyze the GISS dataset by employing a new stochastic dynamical method of time-series analysis that was shown to capture the seasonal variability in monthly-averaged temperature data from decadal to 133 years [25]. This method centers on a periodic non-autonomous stochastic model for the observed deviation in the surface heat flux, $x(t)$, given by $\dot{x} = a(t)x + N(t)\xi(t) + d(\tau)$, where

$a(t)$ and $N(t)$ are periodic functions with annual periodicity, $\xi(t)$ is stochastic noise, and $d(\tau)$ represents decadal forcing. Thus, the first two terms in the model explain the seasonal variability and the last term $d(\tau)$ captures the trans-seasonal variability. The approach provides analytical expressions for $a(t)$, $N(t)$ and $d(\tau)$, and reproduces the observed monthly statistics (Fig. 1 of [25].)

Second, we employ MF-TW-DFA to analyze the annual time-series for each latitude-longitude pair from the GISS dataset. A dominant signal at all locations is the presence of pink noise behavior ($\beta \approx 1$) on multi-decadal timescales. Pink noise, often referred to as "ubiquitous noise" [e.g., 12–17], is observed in a wide range of systems, such as earthquakes, stellar luminosity, electronics, and climate on a variety of time scales [e.g., 14]. We quantify the spatial structure of this statistical behavior by showing the timescales on a global map; Fig. 1 shows the shortest timescale (in years) at which pink noise behavior appears in the data. Latitude-longitude pairs that do not show such behavior are shown in red, while points where no data was present are left blank. Time scales greater than about 60 years are constrained by the finite length of the dataset. Thus, the colors on Fig. 1 have two interpretations; pink noise from 1 to 60 years but no pink noise for longer times. Because both $d(\tau)$ and annual averaging of the data represent different forms of temporal filtering, they exhibit similar timescales for the global appearance of pink noise behavior, but we find quantitative but not qualitative differences [20]. However, the value of using $d(\tau)$ is that it embodies the effects of seasonal stability and noise on annual and longer time scales. The point-wise values of $d(\tau)$ in the GISS dataset exhibit pink noise characteristics on decadal and multi-decadal timescales nearly everywhere on the globe. Dominant global climate variability phenomena such as the El Niño-Southern Oscillation (ENSO) immediately emerge from this analysis. ENSO has been studied extensively and shown to influence global climate on time scales ranging from inter-annual to multi-decadal through atmospheric and oceanic teleconnections [e.g., 26]. This phenomenon has also been related to global rainfall, a driver of global natural climate variability, which is a response to the regional amount of precipitation and evaporation, reflecting the variability in surface heat flux.

To examine the spatial structure of $d(\tau)$, and whether it captures the principal contributions to decadal variability, we construct two one-point correlation maps. As seen in Fig. 2, $d(\tau)$ nearly mirrors two key decadal variability indices; (a) the Pacific Decadal Oscillation (PDO) [6] and (b) the North Atlantic Oscillation (NAO) [27]. We use Empirical Orthogonal Function (EOF) analysis [28] to determine the dominant spatial pattern. Fig. 2(c) shows the first EOF mode and explains 21% of the total variance, with the rest of the modes characterized by shorter timescales [20]. This first mode connects the major PDO region in the eastern Pacific to the Southern Ocean region (also seen in simulations [29]), and is very similar to the so-called "hyper climate modes" [30] and the "Inter-decadal Pacific Oscillation" (IPO) [8] in the Pacific Ocean. The time-series of the Principal Component (PC) shows clear multi-decadal variability. We note that the sign of the mode changes from positive to negative at about the start of the new millennium. A negative sign denotes the intensification of the negative PDO in the North Pacific and the cooling of the Southern Ocean circumpolar region. Simulations [1, 3] have shown that the cooling of the eastern tropics is correlated with the "global warming hiatus" and the average sea surface temperature trends from ten climate models, which capture the hiatus, are negative in the Eastern Pacific and Southern Ocean [4]. The leading EOF of $d(\tau)$ introduced here may be related to this hiatus. Fig. 2(d) shows the result of MF-TW-DFA using the time-series of the PC; the onset of pink noise behavior occurs after approximately 15-years, indicated by the fluctuation function mirroring the red dashed line denoting $\beta = 1$. This noise behavior and its global presence on multi-decadal timescales raises the natural question; is pink noise dynamics an internal feature of the multi-decadal variability of our climate, or imprinted on the climate system by anthropogenic forcing? We address this question by analyzing paleoclimate proxies.

FIG. 1: Spatial distribution of the shortest timescale (in years) at which pink noise behavior appears in the GISS dataset. This transition takes place on multi-decadal timescales nearly everywhere. The red color denotes locations that do not show pink noise characteristics on timescales up to 65 years (half of total length of the dataset), with the most prominent feature being in the tropical eastern Pacific. White regions show locations where continuous data are absent.

Paleoclimate studies have been broadly successful in observing the long-term evolution and variability of Earth's climate [e.g. 31, 32]. Due to their comparatively high resolution, we focus on the proxy data from speleothems and ice cores to (a) understand the observed pink signal in the GISS data, and (b) study the effect of anthropogenic climate change on natural climate variability. Our datasets cover a substantial swath of the globe; Asia, Europe, North America, Central America, South America, and Antarctica along with the Pacific Islands [20]. These data provide a long record of Earth's

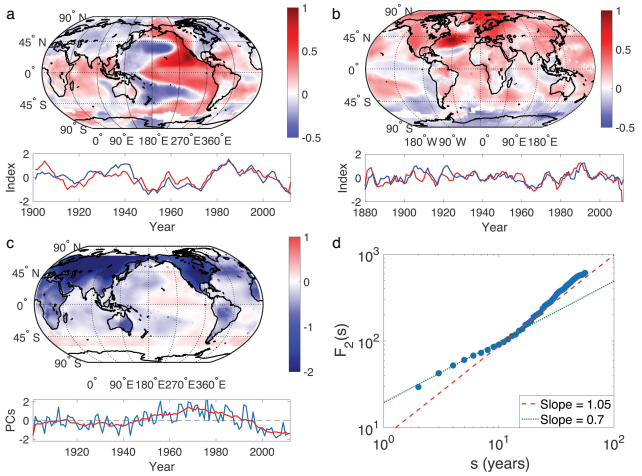

FIG. 2: Spatial distribution of the values of $d(\tau)$ represented by one-point correlation maps and an Empirical Orthogonal Function (EOF) analysis using the Goddard Institute for Space Studies (GISS) surface monthly-averaged temperature from 1901 to 2012. Centered in the eastern Pacific at 120W, 20N, we calculate the correlation between the $d(\tau)$ at this position and that at any other position (a). The spatial distribution of the correlation is nearly identical to the dipole mode called the Pacific Decadal Oscillation (PDO) [1]. The newly constructed index (red), the normalized value of $d(\tau)|_{120W,20N} - d(\tau)|_{180E,40N}$, is compared with the traditional normalized PDO index (blue), which shows an excellent match. A similar one-point correlation map is constructed based on the geographic position at 50W, 38N and is shown in (b). This map is very similar to the SST pattern in the negative state of the NAO [19], as shown by the correlation between $d(\tau)|_{50W,38N} - d(\tau)|_{40W,50N}$ (red) and the normalized NAO index (blue). The EOF analysis is applied to the values of $d(\tau)$, with the leading mode explaining 21% of the total variance, as shown in (c), along with the Principal Component (PC). This mode connects the major PDO region in the eastern Pacific to the Southern Ocean through a continuous same-sign region, as distinguished from the other areas. The time-series of the principle component of the mode is analyzed using MF-TW-DFA (d). At lower frequencies the variability of $d(\tau)$ parallel's pink noise (red dashed line, $\beta = 1$), with a crossover time of ≈ 15 years.

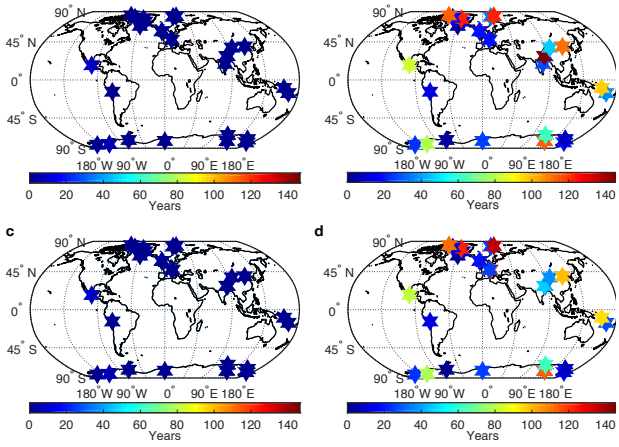

FIG. 3: The initial (a,c) and final (b,d) timescales exhibiting pink noise dynamics in the paleoclimate data across the globe [20], where a & b (c & d) show the analysis for the complete dataset (after removing data from 1850-present), to enable us to distinguish between natural climate variability and anthropogenic forcing. There are no discernible differences between (a,b) and (c,d), implying that pink noise dynamics are an internal characteristic of the Earth's climate system.

climate system, drawing from many sources dating back more than 100,000 years. Figure 3(a) shows the fluctuation functions for the paleoclimate proxy data from various sources [20]. Two things are immediately evident: nearly all datasets show consistent pink noise behavior, and, as was observed in the GISS dataset, the transition timescale to this behavior depends on geographic location.

To study the impact of anthropogenic forcing on internal climate variability and the observed pink noise behavior, we use MF-TW-DFA to analyze only data up to 1850 A.D. Figure 3 shows that the fluctuation functions with and without the post-industrial period exhibit very little difference, indicating that the observed pink noise behavior is intrinsic to Earth's climate dynamics. In data from the last 80,000 years, we also find a timescale of approximately 1470 years (Fig. 4), the signal often ascribed to Dansgaard-Oeschger (DO) events [32]. We hypothesize the possibility of a stochastic resonance process due to the presence of pink noise on multi-decadal timescales as follows. Nozaki and Yamamoto [33] showed that for noise with $1/f^{\beta}$, $0 \leq \beta \leq 2$, the noise intensity for which resonance takes place is *minimized* when $\beta \approx 1$ for relaxation oscillator dynamical systems, and DO events exhibit relaxation oscillation behavior [34, 35]. Thus, the resonance efficiency is *maximal* for $\beta \approx 1$, and in all of these proxies DO events are preceded by pink noise on multi-decadal to centennial timescales, suggesting a much smaller pink noise intensity can lead to a new climatic state relative to other noise types, such as white noise. Importantly, whether the DO events arise from stochastic resonance, a "ghost-resonance" or a related process is actively debated [e.g., 35–40], and here we emphasize that the time scale emerges from a stochastic data analysis method with no assumptions regarding periodicity. We note further that in the dust flux data, which spans the last 800,000 years, we see a clear periodic 100,000-year signal related to the Milankovitch eccentricity cycle, providing a fidelity check for our methodology.

Proxies such as $\delta^{18}O$ and $\delta^{13}C$, from ice-cores and speleothems, are used to infer past temperature, amongst other climate variables. Because temperature reflects heat flux at a given location, such flux dependent quantities are key mirrors of the climate system. In the low (high) latitudes, heat fluxes drive precipitation-evaporation (freezing-melting). Thus, global moisture fluxes are reflected with high fidelity in the ice core and speleothem proxy data and thereby encode aspects of climate variability. For example, ENSO underlies major global rainfall patterns through atmospheric and oceanic teleconnections. Importantly, there are regional differences in the timescales over which the various paleoclimate proxies exhibit pink noise. Each precipitation-

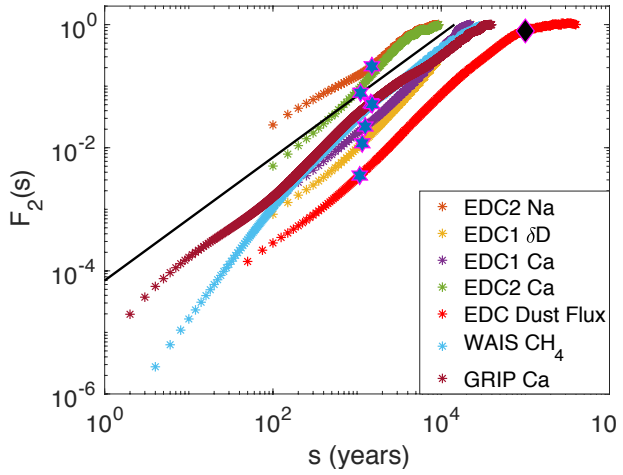

FIG. 4: Fluctuation functions $F_2(s)$ for paleoclimate proxy data (see inset and Table I in [20]) spanning at least the past 80,000 years. The red stars show the crossover timescale of $\sim$ 1470 years, associated with Dansgaard-Oeschger events. For reference, the black diamond denotes the 100,000 year Milankovitch eccentricity cycle, the time scale of Late Pleistocene glaciations. The black line has a slope of unity ($\beta = 1$).

based proxy depends on the net heat flux at a given location and hence we expect regional variability of the pink noise timescales.

Analysis of Sea Surface Temperature (SST) data has also revealed pink noise in the mid-latitudes [41], rationalized by a simple vertical diffusion model with a shallow mixed layer forced by random atmospheric motions [42]. Essential here is the accumulation of the response from random atmospheric forcing due to the large heat capacity of ocean. This local variability in the mid-latitude and tropical oceans is transferred to the global scale via atmospheric teleconnections and ocean waves [26, 43]. Here, this is reflected in our first EOF mode with a time evolution that shows pink noise statistics on multi-decadal time-scales. Moreover, the IPO, which we have shown mirrors our first EOF mode, is strongly linked to global precipitation [43], consistent with the relationship between the pink noise behavior found in the proxies that reflect precipitation and the EOF mode.

Kendal and Jørgensen [13] have shown that both pink noise and fluctuation scaling (wherein the variance of a sequence of observations x is related to the mean by a power law; $\mathrm{Var}(x) \propto \bar{x}^b$) imply each other and can be explained by a central limit-like convergence theorem that establishes which Tweedie exponential dispersion models act as foci for this convergence [44]. The duality between fluctuation scaling and pink noise not only provides a universal treatment of the statistics of the global mode that emerges from this wide range of data we have studied, but a common understanding of their non-Gaussianity.

We note that the intrinsic nature of both the first EOF mode and the pink noise behavior suggest the intriguing potential of a resonance with external low-frequency forcing, such as that associated with anthropogenic effects. Such a resonance may underlie processes associated with global warming hiatus, emphasizing the importance of understanding internal multi-decadal variability.

Finally, non-autonomous stochastic differential equations constitute a key organizing center of our approach [25], and they are also central to the so-called supersymmetric theory of stochastics [e.g., 45, 46]. That approach argues that pink noise is a manifestation of the spontaneous breakdown of topological supersymmetry. However, to ascribe the associated Goldstone modes to specific climate processes is too speculative at present, although the breaking of time-reversal symmetry by Earth's rotation has been shown to provide a topological origin for equatorially trapped waves [47]. Therefore, understanding the origin of the emergence the decadal modes in the climate system that we have observed here may be fruitfully pursued along these lines.

ACKNOWLEDGMENTS

WM acknowledges a Herchel-Smith postdoctoral fellowship for support. SA acknowledges David Crighton fellowship for support. SA and JSW acknowledge NASA Grant NNH13ZDA001N-CRYO. JSW and WM acknowledge Swedish Research Council grant no. 638-2013-9243, and JSW a Royal Society Wolfson Research Merit Award for support.

[1] Y. Kosaka and S.-P. Xie, Nature **501**, 403 (2013).
[2] T. R. Karl, A. Arguez, B. Huang, J. H. Lawrimore, J. R. McMahon, M. J. Menne, T. C. Peterson, R. S. Vose, and H.-M. Zhang, Science **348**, 1469 (2015).
[3] K. E. Trenberth and J. T. Fasullo, Earth's Future **1**, 19 (2013).
[4] M. Watanabe, H. Shiogama, H. Tatebe, M. Hayashi, M. Ishii, and M. Kimoto, Nat. Clim. Change. **4**, 893 (2014).
[5] G. A. Meehl, H. Teng, and J. M. Arblaster, Nat. Clim. Change. **4**, 898 (2014).
[6] N. J. Mantua and S. R. Hare, J. Oceanogr. **58**, 35 (2002).
[7] M. E. Schlesinger and N. Ramankutty, Nature **367**, 723 (1994).
[8] M. J. Salinger, J. A. Renwick, and A. B. Mullan, Int. J. Climatol. **21**, 1705 (2001).
[9] T. P. Barnett, Mon. Weather. Rev. **106**, 1353 (1978).
[10] J. Ludescher, M. I. Bogachev, J. W. Kantelhardt, A. Y. Schumann, and A. Bunde, Physica A **390**, 2480 (2011).
[11] S. Agarwal, W. Moon, and J. S. Wettlaufer, Proc. R. Soc. A **468**, 2416 (2012).
[12] J. Davidsen and H. G. Schuster, Phys. Rev. E **65**, 026120 (2002).
[13] W. S. Kendal and B. Jørgensen, Phys. Rev. E **84**, 066120

(2011).
[14] R. Blender, X. Zhu, and K. Fraedrich, Adv. Sci. Res. **6**, 137 (2011).
[15] M. Niemann, H. Kantz, and E. Barkai, Phys. Rev. Lett. **110**, 140603 (2013).
[16] J. Herault, F. Petrelis, and S. Fauve, EPL **111**, 44002 (2015).
[17] M. Brownnutt, M. Kumph, P. Rabl, and R. Blatt, Rev. Mod. Phys. **87**, 1419 (2015).
[18] GISTEMP-Team, *GISS Surface Temperature Analysis (GISTEMP)*, NASA Goddard Institute for Space Studies. Dataset accessed 2017-01-15 (2017).
[19] J. Hansen, R. Ruedy, M. Sato, and K. Lo, Rev. Geophys. **48**, RG4004 (2010).
[20] *See Supplemental Material for a description of the datasets used, MFTWDFA, statistical analysis of exponents, stochastic time-series analysis method, and the EOF method and includes Refs. [48, 49].*
[21] Y. Zhou and Y. Leung, J. Stat. Mech.-Theory & Experiment **2010**, P06021 (2010).
[22] S. Agarwal and J. S. Wettlaufer, J. Clim. **30**, 4873 (2017).
[23] S. Agarwal, F. D. Sordo, and J. S. Wettlaufer, Astron. J. **153**, 12 (2017).
[24] O. Løvsletten, Phys. Rev. E **96**, 012141 (2017).
[25] W. Moon and J. S. Wettlaufer, Sci. Rep. **7**, 44228 (2017).
[26] Z. Liu and M. Alexander, Rev. Geophys. **45**, RG2005 (2007).
[27] H. Wanner, S. Brönnimann, C. Casty, D. Gyalistras, J. Luterbacher, C. Schmutz, D. B. Stephenson, and E. Xoplaki, Surv. Geophys. **22**, 321 (2001).
[28] E. N. Lorenz, *Empirical orthogonal functions and statistical weather prediction*, Tech. Rep. (Department of Meteorology, MIT, 1956).
[29] D. L. Bars, J. P. Viebahn, and H. A. Dijkstra, Geophys. Res. Lett. **43**, 2102 (2016).
[30] D. Dommenget and M. Latif, Geophys. Res. Lett. **35**, L02706 (2008).
[31] J. Zachos, M. Pagani, L. Sloan, E. Thomas, and K. Billups, Science **292**, 686 (2001).
[32] W. Dansgaard, S. J. Johnsen, H. B. Clausen, D. Dahl-Jensen, N. S. Gundestrup, C. U. Hammer, C. S. Hvidberg, J. P. Steffensen, A. E. Sveinbjornsdottir, J. Jouzel, and G. Bond, Nature **364**, 218 (1993).
[33] D. Nozaki and Y. Yamamoto, Phys. Lett. A **243**, 281 (1998).
[34] A. Timmermann, H. Gildor, M. Schulz, and E. Tziperman, J. Clim. **16**, 2569 (2003).
[35] N. Boers, M. D. Chekroun, H. Liu, D. Kondrashov, D.-D. Rousseau, A. Svensson, M. Bigler, and M. Ghil, Earth Syst. Dynam. **8**, 1171 (2017).
[36] C. Wunsch, Paleoceanography **15**, 417 (2000).
[37] P. D. Ditlevsen, M. S. Kristensen, and K. K. Andersen, J. Clim. **18**, 2594 (2005).
[38] P. Balenzuela, H. Braun, and D. R. Chialvo, Contemp. Phys. **53**, 17 (2012).
[39] S. Krumscheid, M. Pradas, G. A. Pavliotis, and S. Kalliadasis, Phys. Rev. E **92**, 042139 (2015).
[40] M. Rypdal, J. Clim. **29**, 4047 (2016).
[41] K. Fraedrich and R. Blender, Phys. Rev. Lett. **90**, 108501 (2003).
[42] K. Fraedrich, U. Luksch, and R. Blender, Phys. Rev. E **70**, 037301 (2004).
[43] B. Dong and A. Dai, Clim. Dynam. **45**, 2667 (2015).
[44] B. Jørgensen, J. R. Martinez, and M. Tsao, Scand. J. Stat. **21**, 223 (1994).
[45] I. V. Ovchinnikov, Chaos **22**, 033134 (2012).
[46] I. V. Ovchinnikov, Entropy **18**, 108 (2016).
[47] P. Delplace, J. B. Marston, and A. Venaille, Science **358**, 1075 (2017).
[48] P. Huybers and W. Curry, Nature **441**, 329 (2006).
[49] Z. G. Shao and P. D. Ditlevsen, Nature Comm. **7**, 10951 (2016).